Int. J. Electrochem. Sci., 15 **(2020)** 4406 – 4420, doi: 10.20964/2020.05.32

International Journal of
ELECTROCHEMICAL
SCIENCE
www.electrochemsci.org

Effect of pH on the Passive Film Characteristics of Lean Duplex Stainless Steel in Chloride-Containing Synthetic Tap Water

Sangwon Cho[1], *Jeong-Hun An*[1], *Seung-Hwan Lee*[2], *Jung-Gu Kim*[1,*]

[1] Department of Materials Science and Engineering, Sungkyunkwan University, 2066, Seobu-Ro, Jangan-Gu, Suwon-Si, Republic of Korea, 16419
[2] Steel Solution Marketing Dept., POSCO Global R&D Center, 100, Songdogwahak-Ro, Yeonsu-Gu, Incheon, Republic of Korea, 21985.
[*]E-mail: kimjg@skku.edu

Received: 25 October 2019 / *Accepted:* 18 December 2019 / *Published:* 10 April 2020

The localized corrosion properties of lean duplex stainless steel and 316L stainless steel were compared using electrochemical testing and angle resolved X-ray photoelectron spectroscopy analysis. Electrochemical testing at pH 7 revealed that the pitting corrosion resistance of LDSS was superior to that of 316L, but the crevice corrosion resistance of 316L was better than that of LDSS. In potentiodynamic polarization testing, as the pH decreased, the pitting potential of 316L did not change significantly. However, the pitting potential of LDSS sharply decreased with decreasing pH, and was lower than that of 316L at pH 2. Electrochemical impedance spectroscopy results confirmed that the passive film of 316L is more stable than that of LDSS at lower pH. Regardless of the pH and film depth, the passive film compositions of 316L and LDSS were similar, except for Mo compounds. Mo peaks were not detected in either steel at pH 7, but pronounced spectra of the Mo were detected only for the 316L steel at pH 2. Mo oxides are not formed at a neutral pH, but formed at lower pH. The improved resistance to crevice corrosion of 316L resulted from the formation of the Mo-enriched passive film at low pH.

Keywords Lean duplex stainless steel, Pitting corrosion, Crevice corrosion, Passive film, ARXPS

1. INTRODUCTION

District heating systems provide heat for the inhabitants of large cities, having various advantages such as reduced air pollution, relatively high energy efficiency and reduced life-cycle costs [1,2]. This system consists of three parts: a heat source, a distribution system and a customer interface. Between each part, shell-and-tube type and plate type heat exchangers are installed, which supply the produced heat to the customer interface. Austenitic stainless steels are mainly used as materials for the plate heat exchanger installed between the distribution system and the customer interface, due to their good

corrosion resistance [3-5]. This heat exchanger is usually damaged by high-temperature heating water containing chloride ions, which can lead to unexpected failure. Damage to the plate heat exchanger mostly occurs through the tap water on the customer interface side, and failure is usually the result of pitting corrosion and cracking due to crevice corrosion between the gasket and the heat exchanger [3,4,6].

Pitting corrosion and crevice corrosion are similar in many respects. For example, the influences of alloying elements and the environment on corrosion resistance are the same for pitting and crevice corrosion, and both types of corrosion have critical threshold potential [7,8]. However, there are some distinct differences, one of which is the initiation mechanism (i.e., the initiation site and change of pH). For crevice corrosion, hydrogen ions are generated by a hydrolysis reaction involving metal ions inside the crevice, and a major feature is that the pH decreases continuously until it becomes almost zero [8-10]. At that point, when the pH inside the crevice reaches the depassivation pH (pHd), the passive film breaks down and crevice corrosion begins. In the case of crevice corrosion of stainless steel, the depassivation pH is the pH at which the anodic dissolution rate rapidly increases, and depends on the alloying element [8]. The pHd is an index demonstrating the resistance of the passive film to breakdown, and the most important alloying elements determining the pHd are Cr and Mo. If the pH changes, the pitting and crevice corrosion resistance of stainless steel can be changed in various ways [11].

Duplex stainless steels have recently been drawing interest due to their excellent corrosion resistance, mechanical properties and weldability in various environments compared with general stainless steels [12]. Due to these properties, duplex stainless steels have been applied in various industries for petrochemical equipment, offshore structures, power plants and other similar industries [13,14]. However, since duplex stainless steels are expensive, they have the drawbacks of being difficult to implement in places requiring frequent replacement. To deal with these problems, lean duplex stainless steels (LDSS) were developed. Lean duplex stainless steels not only have the same level of formability and corrosion resistance as general stainless steels, but are also are inexpensive because the contents of expensive alloying elements such as nickel and molybdenum are greatly reduced [6,16]. Therefore, the application of lean duplex stainless steel makes it possible to maintain and economically manage equipment requiring frequent replacement, such as heat exchanger plates or heat exchanger tubes. Recently, LDSS was developed as an alternative to 304 stainless steel and 316L stainless steel, and has been applied in various places.

Even though there has been studies on the localized corrosion of austenitic and duplex stainless steels have been actively installed in chloride-containing environments, the research on lean duplex stainless steel has been limited. In this study, the localized corrosion behavior of LDSS was investigated and compared with that of 316L in the operating environment of the plate heat exchanger for a district heating system.

2. EXPERIMENTAL METHODS

Two types of stainless steel, 316L and LDSS, were used in this study and Table 1 lists the chemical compositions of the specimens. For the electrochemical test, the surface of the specimen was

abraded up to #600 with SiC paper, degreased with ethanol and dried with N_2 gas. The test environment was chloride-containing synthetic tap water (450 ppm) at various pHs (7, 6, 4, 2) at 60 ℃. The pH of the solution was adjusted using HCl and NaOH. All measurements were carried out in an aerated condition.

Table 1. Chemical compositions of stainless steels (wt%).

	C	Mn	P	S	Si	Cr	Ni	Mo	Cu	N
316L	0.028	0.95	0.045	0.03	0.048	18.74	9.2	1.96	-	0.1
LDSS	0.060	2.50-3.50	0.040	0.030	0.90	19.5-22.0	0.5-1.5	-	0.20-1.20	0.2-0.3

All electrochemical experiments were performed with a three-electrode electrochemical cell. The counter electrode was a graphite rod, and a saturated calomel electrode was used as a reference electrode. The area exposed to the electrolyte was 1 cm^2. Before polarization, the specimens were cathodically polarized at -1.2 V_{SCE} for 5 min to remove air-formed surface oxides. The open-circuit potential (OCP) was established over the span of 6 h.

Cyclic potentiodynamic polarization (CPP) test and potentiodynamic polarization test were conducted with a potential sweep of 0.166 mV/s in accordance with ASTM G6117 and ASTM G518, respectively. The scan direction was reversed at a current density of 10^{-3} A/cm^2. Based on the standard guidelines for crevice corrosion testing (ASTM G7819), the modified multiple-crevice assembly (MCA) was used. In this assembly, the specimen and two crevice formers are tightened with a bolt, nut, and acetal washer using a torque wrench (8.5 N·m). Potentiostatic polarization tests were carried out at 0.2, 0.3, 0.4 and 0.6 V_{SCE} for 24 hours to examine the tendency of the passive film to break down, as well as confirm the results of the CPP analysis. Electrochemical impedance spectroscopy (EIS) tests were performed with an amplitude of 10 mV in the frequency range of 100 kHz to 1 mHz.

The chemical composition of the passive film was investigated via angle resolved X-ray photoelectron spectroscopy (AR-XPS) with 15°, 45° and 75° take-off angles. For XPS analysis, the passive film layers on the steel surface were formed under potentiostatic conditions for 1 hour at 0.1 V_{SCE}. After electrochemical preparation, the specimens were rinsed with distilled water, dried and transferred to the analyzer chamber.

3. RESULTS AND DISCUSSION

3.1 Pitting Corrosion Resistance Measurement

The cyclic potentiodynamic polarization (CPP) curves and results under non-crevice conditions are shown in Figure 1 and Table 2, respectively. All of the polarization curves exhibited hysteresis. For 316L, a sharp increase in the current density was observed, and the pitting potential (E_{pit}) was obvious. On the other hand, the current density of LDSS tended to increase constantly at a higher potential than

in the passive region; this potential was in a transpassive region in which the protective properties of the passive films were reduced [8]. In addition, a sharp increase in the current density was observed at 1.27 V_{SCE}. From the curves obtained by this test, the pitting potential of 316L and LDSS were determined to be 0.45 V_{SCE} and 1.27 V_{SCE}, respectively. This indicates that the pitting corrosion resistance of LDSS is much better than that of 316L.

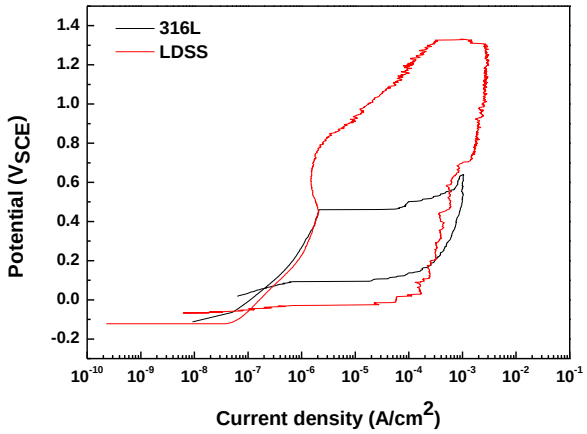

Figure 1. Cyclic potentiodynamic polarization curves for stainless steels in synthetic tap water (pH=7, 60 ℃).

Table 2. Cyclic potentiodynamic polarization test results.

	E_{corr} (mV_{SCE})	E_{pit} (mV_{SCE})	E_{prot} (mV_{SCE})	$E_{prot} - E_{corr}$ (mV_{SCE})
316L	-112	450	-6	106
LDSS	-137	1,273	-95	41

At pH 7 and 60 ℃, the equilibrium potential of the oxygen evolution reaction ($4OH^- \rightarrow O_2 + 2H_2O + 4e^-$) is approximately 525 mV_{SCE}. Thus, the sharp increase of current density at a high potential can be attributed to the oxygen evolution reaction on LDSS. The oxygen generation reaction on the surface of the metal promotes the breakdown of the passive film and facilitates the formation of pitting corrosion. Thus, pitting corrosion is a result of mixed reactions of metal/electrolytes and oxygen generation, and the measured current density is the sum of these reactions [20-22]. In other words, E_{pit} of LDSS cannot be absolute values indicating the pitting corrosion resistance.

The protection potential (E_{prot}) is a potential that measures the tendency of repassivation. The E_{prot} values of the two steels were higher than their corrosion potential (E_{corr}) values. This indicates that both the initiation of new pits and the propagation of already formed pits did not occur [23].

Figure 2 shows the results of the potentiostatic polarization tests under non-crevice conditions. As shown in Figure 2a (E_{app}=0.4 V_{SCE}), the increase in current density was doubled (after 2 minutes and 2 hours) in 316L. Generally, pitting corrosion is thought to occur when the current density reaches 100 $\mu A/cm^2$ [24]. Therefore, the increase in current density at the initial stage was due to the formation of a

metastable pit by repeated formation and repassivation of a micro-size pit [25-27]. The increase in current density in the next stage was due to the initiation of pitting corrosion. After the pitting corrosion was initiated, the current density did not decrease again, indicating that the pit was not repassivated. For LDSS, an increase in current density was not observed within 24 hours. This is because the applied potential was lower than E_{pit} and the stability of the passive film was maintained. In Figure 2b (E_{app}=0.6 V_{SCE}), the current density of 316L and LDSS increased immediately after potential application. The applied potential is higher than the E_{pit} of 316L, and belongs to the transpassive region of LDSS. Thus, the current density of 316L sharply increased as the potential was applied, and repassivation did not occur. In the case of LDSS, incomplete pitting occurred because the applied potential was in the transpassive region, and the current density increased and decreased repeatedly. The initiated pits were repassivated after 7.5 hours.

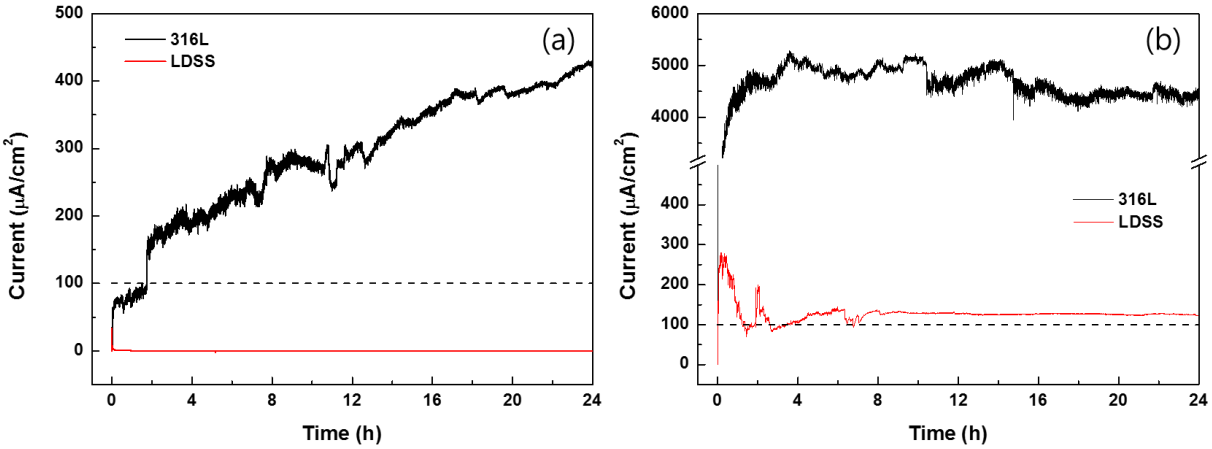

Figure 2. Current variation with time at the applied potentials of (a) 0.4 V_{SCE} and (b) 0.6 V_{SCE} for 24 h in synthetic tap water (pH=7, 60 ℃).

3.2 Crevice Corrosion Resistance Measurement

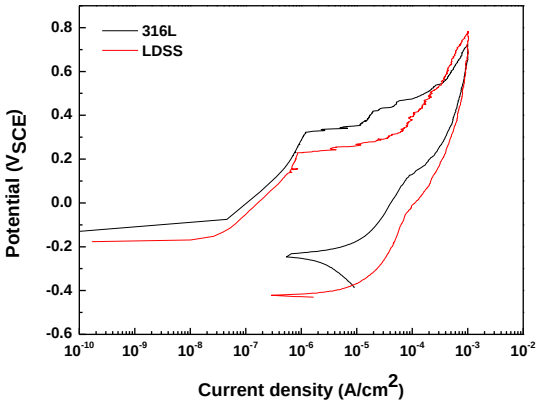

Figure 3. Cyclic potentiodynamic polarization curves for stainless steels under crevice conditions in synthetic tap water (pH=7, 60 ℃)

The CPP curves and results under crevice conditions are shown in Figure 3 and Table 3. All the polarization curves exhibited hysteresis. The current density of both steels increased sharply, and the crevice potential (E_{crev}) was clearly observed. E_{crev} was higher for 316L than for LDSS. For both stainless steels, E_{prot} is lower than E_{corr}; thus, new crevice corrosion cannot be initiated, but old ones can still grow [23].

Table 3. Cyclic potentiodynamic polarization test results under crevice corrosion condition.

	E_{corr} (mV_{SCE})	$E_{crevice}$ (mV_{SCE})	E_{prot} (mV_{SCE})	$E_{prot} - E_{corr}$ (mV_{SCE})
316L	-136	344	-246	-111
LDSS	-177	229	-421	-244

The results of the potentiostatic polarization test for the two steels under crevice conditions are shown in Figure 4. At the applied potential of 0.2 V_{SCE}, the current density of 316L did not change, whereas LDSS showed an increased current density. On the LDSS, metastable localized corrosion occurred. At the applied potential of 0.3 V_{SCE}, the current densities on LDSS are much higher than those on 316L. Thus, two steels could not be repassivated after crevice corrosion occurred [28,29]. Based on the CPP and potentiostatic polarization test results, the crevice corrosion resistance of 316L is better than that of LDSS, unlike the pitting corrosion resistance.

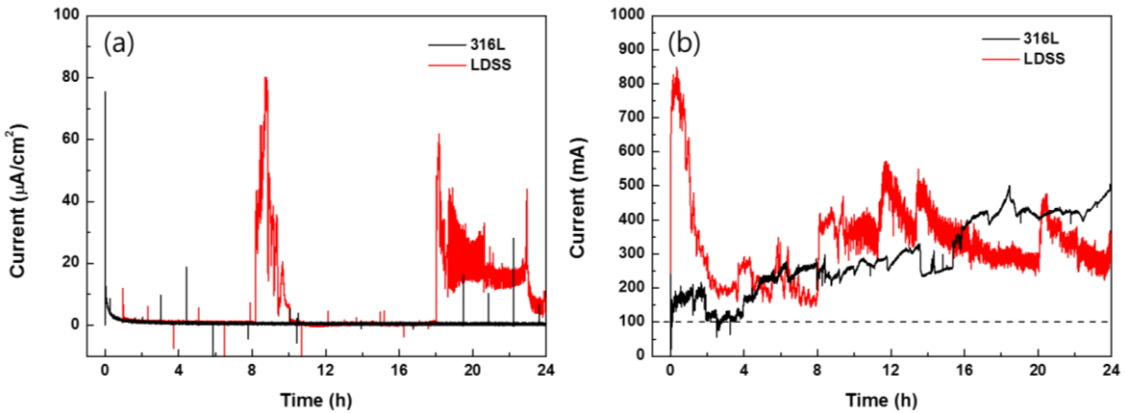

Figure 4. Current variation with time for stainless steels under crevice conditions at the applied potentials of (a) 0.2 V_{SCE} and (b) 0.3 V_{SCE} for 24 h in synthetic tap water (pH=7, 60 ℃).

3.3 Effect of pH on the Passive Film – Electrochemical Analysis

The stability of the passive film with changes in pH was analyzed via anodic potentiodynamic polarization tests of the two steels at various pHs, and the results are presented in Figures 5 and 6. E_{pit} decreased as the pH decreased in both steels. As the pH decreased, E_{pit} decreased more for LDSS than for 316L. This is because the LDSS passive film was more sensitive to pH than 316L. In addition, when

the pH was higher than 2, E_{pit} was higher for LDSS than for 316L, but at pH 2, E_{pit} was higher for 316L than for LDSS.

The results of electrochemical impedance spectroscopy (EIS) in the form of Bode plots according to the pH change are presented in Figure 7. In the Bode plot, high-frequency spectra are associated with defects on the metal surface, whereas low-frequency spectra are related to the surface film and metal/film interface [30-32].

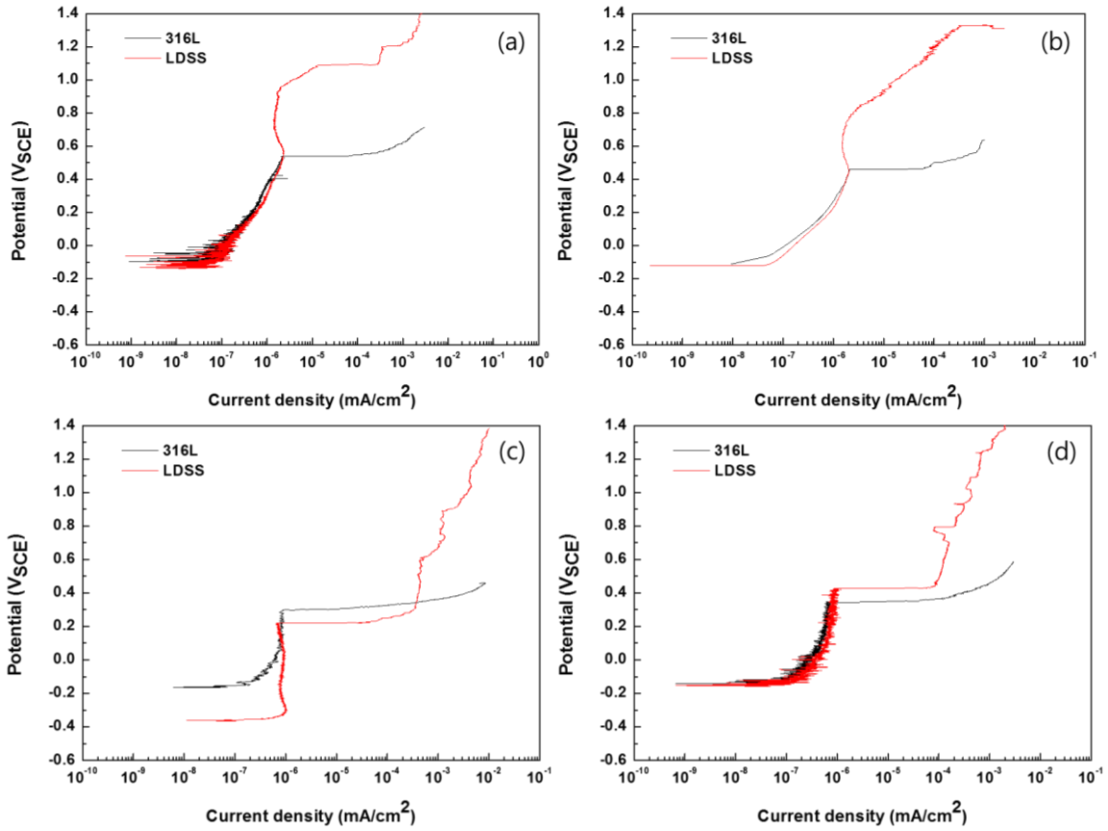

Figure 5. Anodic potentiodynamic polarization curves of (a) pH 7, (b) pH 6, (c) pH 4 and (d) pH 2 in synthetic tap water (60 ℃).

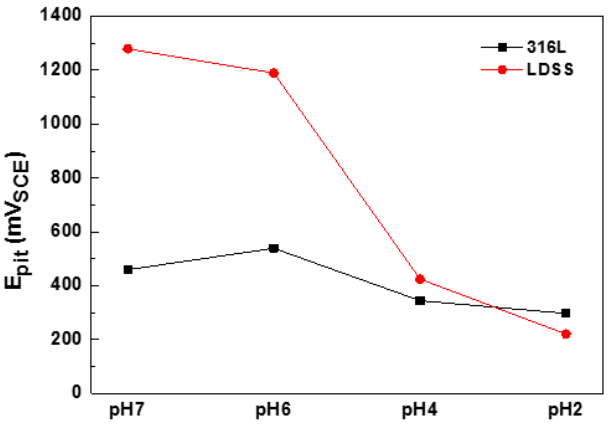

Figure 6. Variation of pitting potential (Epit) according to changes in pH based on the potentiodynamic anodic polarization test results.

The phase angle maxima were equal for the two steels regardless of the pH, and decreased slightly in both steels as the pH decreased. This is due to the existence of a porous passive film [33]. Consequently, degradation of the passive film was accelerated as the pH decreased. The shoulder width of the phase angle of LDSS was larger than that of 316L at pH 7, whereas that of 316L was larger than LDSS at pH 2. This indicates that the passive film stability of 316L is superior to that of LDSS at low pH.

Figure 8 shows the equivalent circuit used to determine the optimized values for the capacitance and resistance parameters [34,35]. R_s is the solution resistance, and CPE1 and R_{film} are the passive film capacitance and resistance, respectively. CPE2 is the double-layer capacitance generated by the dissolution of the metal and the charge separation between the metal and the electrolyte interface, and R_{ct} is the charge transfer resistance [33,34]. The impedance of CPE is expressed by the following equation:

$$Z_{CPE} = A^{-1}(i\omega)^{-n} \quad (1)$$

where Z is the impedance, A is the coefficient of proportionality, *i* is the imaginary number, ω is the angular frequency, and n is an empirical exponent ($0 \leq n \leq 1$) measuring the deviation from the behavior of an ideal electric capacity [36,37].

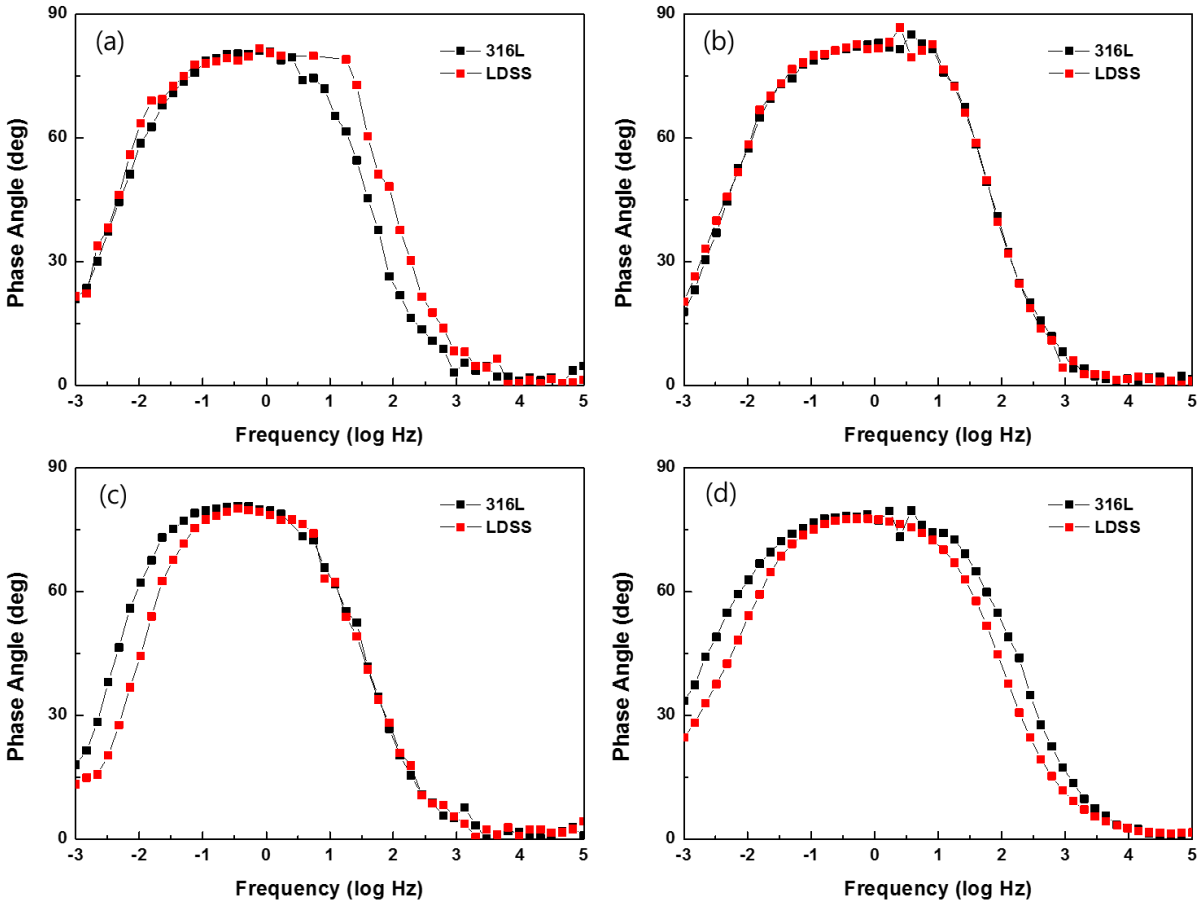

Figure 7. Bode impedance plots of EIS data of (a) pH 7, (b) pH 6, (c) pH 4 and (d) pH 2 in synthetic tap water (60 ℃).

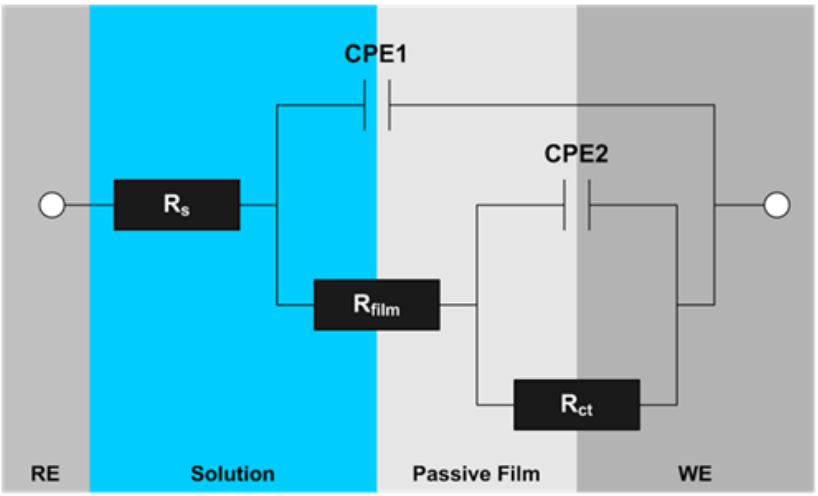

Figure 8. Equivalent circuit for stainless steel in synthetic tap water.

Table 4. Electrochemical impedance spectroscopy results according to pH.

pH	Material	CPE1		R_{film} ($M\Omega/cm^2$)	CPE2		R_{ct} ($M\Omega/cm^2$)
		Q_{film} ($\mu F/cm^2$)	n_1		Q_{ct} ($\mu F/cm^2$)	n_2	
7	**316L**	38.9	0.92	45.05	17.39	0.62	42.12
	LDSS	8.75	0.91	48.43	2.83	0.72	3.67
6	**316L**	36.2	0.94	32.94	7.463	0.54	51.91
	LDSS	36.6	0.94	38.94	15.09	0.72	60.33
4	**316L**	50.83	0.92	39.85	27.42	0.56	70.61
	LDSS	56.25	0.91	32.80	2,664	0.90	16.28
2	**316L**	105.8	0.87	37.33	296.8	0.70	27.30
	LDSS	8.559	0.87	8.67	925.7	0.92	0.16

Table 4 presents the optimized values for the capacitance and resistance parameters according to pH change from the EIS test results. The R_{film} of 316L did not change significantly with pH change, whereas the R_{film} of LDSS decreased as the pH decreased. At the lower pH, the R_{film} of LDSS was much lower than that of 316L. In other words, the passive film of LDSS lost its protective properties more easily than that of 316L as the pH decreased. This result is in agreement with that of the potentiodynamic polarization test. Thus, the pitting corrosion resistance of LDSS is better than that of 316L, while the reverse is the case under crevice conditions.

3.4 Effect of pH on the Passive Film – AR-XPS Analysis

The composition of the passive film with a film depth that formed potentiostatically at 0.1 V_{SCE} was analyzed via angle-resolved X-ray photoelectron spectroscopy (AR-XPS). Figures 9 and 10 show the XPS spectra of the passive films on 316L and LDSS at different pHs with various take-off angles. The binding energies of the peaks for the same elements in each passive film were unchanged regardless of the take-off angle. However, the intensity of the XPS spectra weakened as the take-off angle become smaller. This is because a small amount of signal was collected from the more horizontally-oriented take-off angle.

Figure 11 displays the atomic concentration of elements analyzed from the AR-XPS results for different passive films. Even if the take-off angle changes, the concentration of Fe and Cr oxide is similar. In other words, the internal and external compositions of each passive film are almost the same. However, the main component of the passive film in each specimen is different depending on the pH. Fe oxide is dominant in both steels at pH 7, but Cr oxide is more dominant at pH 2. In particular, the amount of Mo oxide at pH 2 increased significantly compared to pH 7.

Figure 12 presents the XPS spectra of Cr, Fe, O, Mo, Mn and Ni obtained at the take-off angle of 45°. In Figures 12a-c, the passive film components of 316L and LDSS were the same regardless of the pH. However, the intensities of the obtained peaks differed according to the pH in both steel types. Because the peak intensity is proportional to the concentration of constituents, these results indicate that the concentrations of the passive film components differed according to the pH [38].

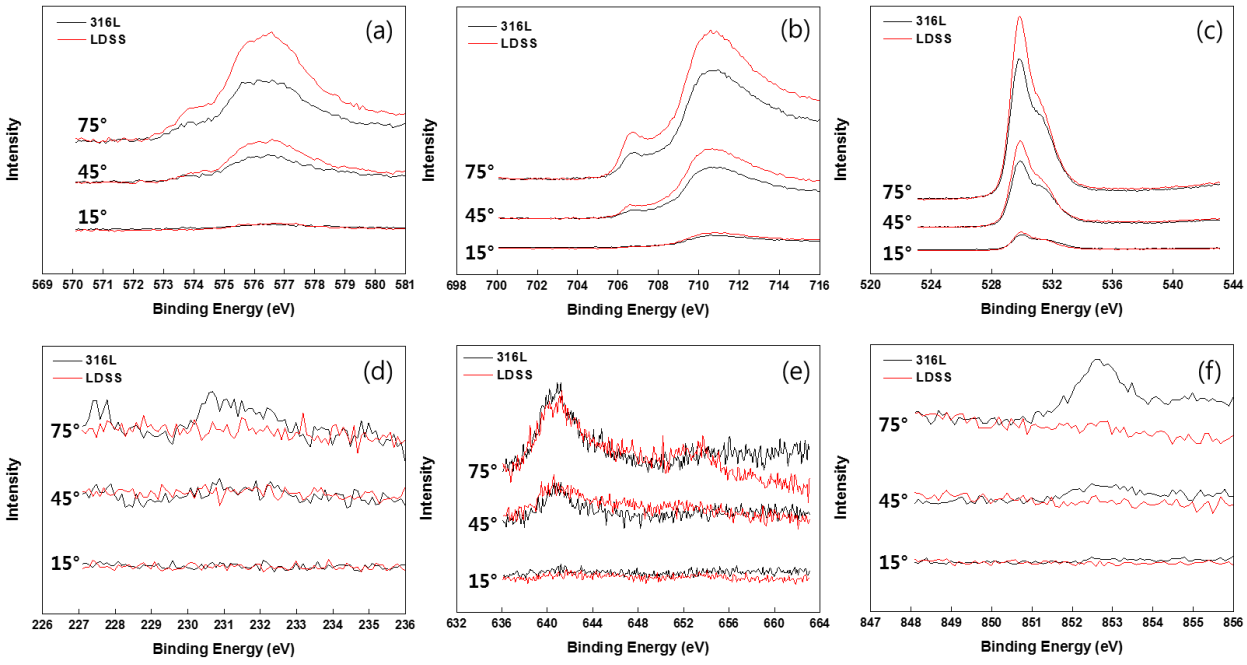

Figure 9. AR-XPS spectra of (a) Cr $2p_{3/2}$, (b) Fe $2p_{3/2}$, (c) O 1s, (d) Mo 3d, (e) Mn 2p, and (f) Ni $2p_{3/2}$ of the passive film formed at 0.1 V_{SCE} for 1 h with various take-off angles (pH=7).

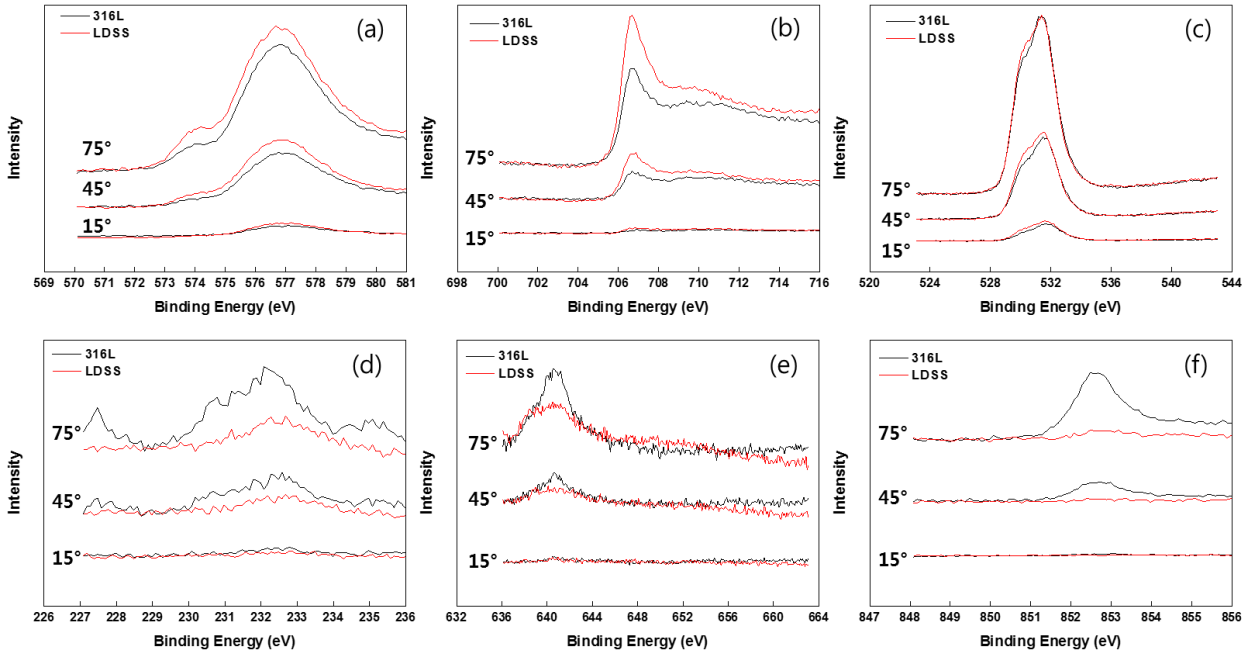

Figure 10. AR-XPS spectra of (a) Cr $2p_{3/2}$, (b) Fe $2p_{3/2}$, (c) O 1s, (d) Mo 3d, (e) Mn 2p, and (f) Ni $2p_{3/2}$ of the passive film formed at 0.1 V_{SCE} for 1 h with various take-off angles (pH=2).

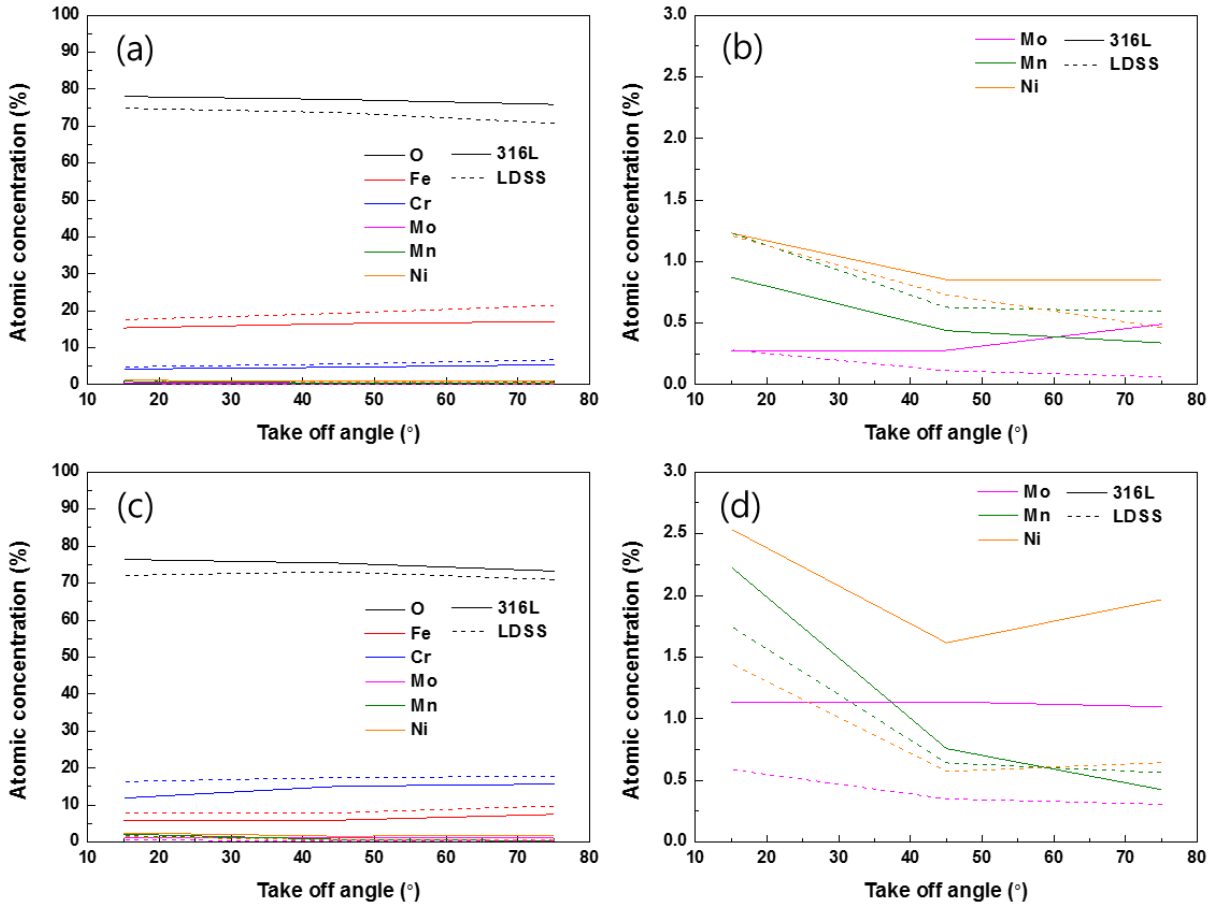

Figure 11. Atomic concentration of passive film; (a)(b) pH 7, (c)(d) pH 2.

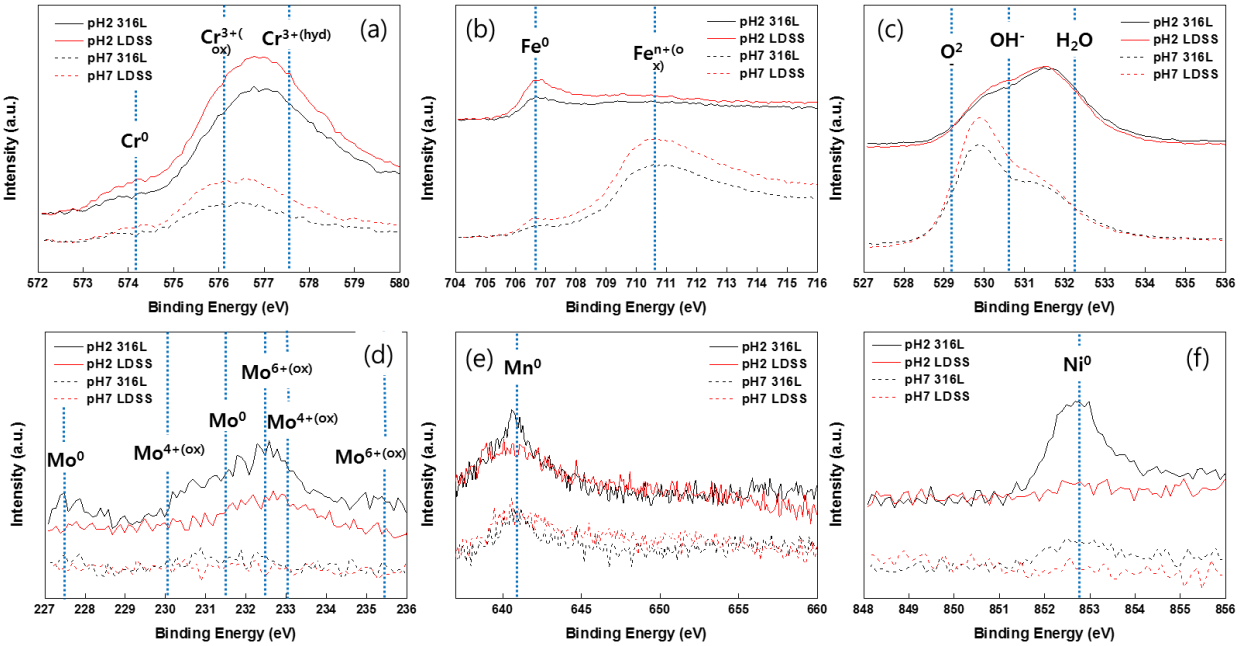

Figure 12. AR-XPS spectra of (a) Cr $2p_{3/2}$, (b) Fe $2p_{3/2}$, (c) O 1s, (d) Mo 3d, (e) Mn 2p, and (f) Ni $2p_{3/2}$ of the passive film formed at 0.1 V_{SCE} for 1 h with 45° take-off angle.

In Figure 12a, Cr (metal), Cr_2O_3 and $Cr(OH)_2$ peaks were presented and their intensities were higher at pH 2 than at pH 7. In Figure 12b, although oxidized Fe $2p_{3/2}$ spectra were deconvoluted to multiple peaks matching individual chemical states in many studies, we considered oxidized Fe $2p_{3/2}$ as a single chemical state because the peak positions of the reported individual components were different depending on the literature [39-44]. The dashed lines in Figure 12b are the peak positions of the metallic and oxidized elements. Fe (metal) and various Fe oxide peaks are shown in Figure 12b. The Fe oxide peak was predominant at pH 7, while the Fe (metal) peak was predominant at pH 2. The O 1s spectra can deconvolute into three elements: O^{2-}, OH^- and H_2O. This indicates that the principal components in the passive layer are metallic oxides and hydroxides. In Figure 12c, the peak intensity of O^{2-} was greater than that of OH^- at pH 7, whereas the peak intensity of O^{2-} was weaker than that of OH^- at pH 2. This indicates that Fe oxide was the main component of the passive film at pH 7, while Cr oxide and hydroxide were the main components at pH 2. In the case of Mo, no peaks were detected for LDSS at pH 2 and in both steels at pH 7, but all the peaks were detected for 316L at pH 2. Mo is well known as an element that greatly improves the localized corrosion resistance of stainless steel in chloride-containing environments [43-47]. Thus, the difference in protective properties of the passive films of the two steels as the pH varied can be attributed to the difference in Mo content. This is clear evidence that Mo contributes to the stability of the passive film on 316L at low pH. In the case of Mn and Ni, atomic concentration signals are collected by Mn (metal) and Ni (metal) from the substrate, not oxides, as shown in Figures 12e and f. Mn (metal) peak was observed on both steels regardless of pH. Since the XPS signal of the Mn ion inside the oxide was too small to be analyzed, it is assumed that the Mn ion did not exist or that a very small amount was present in the passive film. A Ni (metal) peak was observed on 316L regardless of pH, while significant peaks were not detected for LDSS due to the small amount of

Ni. Since the XPS signal of the Ni ion inside the oxide was too small to be analyzed for 316L, it is assumed that the Ni ion did not exist or that a very small amount was present in the passive film. In general, it has been reported that Ni ions in oxides are rarely observed, even when the Ni content is 8% or greater [48,49].

4. CONCLUSIONS

In this study, the localized corrosion properties of lean duplex stainless steel and 316L were compared in chloride-containing synthetic tap water at various pHs via electrochemical tests, and the characteristics of the passive film were analyzed by XPS. The conclusions based on the above investigation are as follows:

- The pitting corrosion resistance of LDSS is better than that of 316L, but the crevice corrosion resistance of LDSS is lower than that of 316L. Under non-crevice conditions, LDSS exhibits transpassive behavior and E_{pit} is greater than the oxygen evolution potential. The E_{prot} values of both steels are higher than E_{corr}. On the other hand, under crevice conditions, E_{prot} is lower than E_{corr} for both steels. Comparative analysis of the localized corrosion resistance by potentiostatic polarization testing agreed with the results of CPP testing.
- E_{pit} tends to decrease as the pH decreases for both steels. The E_{pit} of LDSS sharply decreases below pH 4, and the E_{pit} of LDSS is lower than that of 316L at pH 2. The R_{film} of 316L remains similar even as the pH changes, whereas that of LDSS decreases as the pH decreases. Thus, regardless of the pH, the passive film of 316L maintains its stability, while that of LDSS easily loses its protective properties as the pH decreases.
- Regardless of the pH and film depth, the passive film compositions of the two steels are similar, except for Mo. Fe oxide is the main constituent of the passive film at pH 7, but Cr oxide and hydroxide are the main components at pH 2. And the amount of Mo oxide at pH 2 increased significantly compared to pH 7. For both steels, the peaks of Mo are detectable only at pH 2 and not at pH 7. The Mo peak intensities are much smaller for LDSS than for 316L at pH 2. Thus, the difference in the passive film stability of two steels during pH variation can be attributed to the difference in Mo content.
- Mo oxides are not formed at a neutral pH, but instead at a lower pH. The Mo oxide can easily act as a passive film under the crevice condition. Although pitting and crevice corrosion are similar in many respects, the tendencies of pitting and crevice corrosion resistance can change depending on the concentration of Mo oxide in the passive film.

ACKNOWLEDGMENTS
This research was supported by POSCO.

References

1. D.Y. Lee, W.C. Kim and J.G. Kim, *Corros. Sci*., 64 (2012) 105.
2. S.Y. Choi, K.Y. Yoo, J.B. Lee, C.B. Shin and M.J. Park, *Appl. Therm. Eng*., 30 (2010) 2067.

3. K. M. Deen, M.A. Virk, C.I. Haque and I.H. Khan, *Eng. Fail. Anal*., 17 (2010) 886.
4. S.H. Kim, J.H. Lee and J.G. Kim, *Met. Mater. Int*., 24 (2018) 516.
5. M.M. Abu-Khader, *Adv. Mater. Res. Switz*., 16 (2012) 1883.
6. A. Gagliardi, A. Lanzutti, M. Simonato, R. Furlanetto, M. Magnan, F. Andreatta and L. Fedrizzi, *E ng. Fail. Anal.*, 92 (2018) 289.
7. A.U. Malik, S. Ahmad, I. Andijani and S. Al-Fouzan, *Desalination*, 123 (1999) 205.
8. B. Cottis, M. Graham, R. Lindsay, S. Lyon, T. Richardson, D. Scantlebury and H. Stott, *Shreir's C orrosion: Vol. 2 Corrosion in Liquids, Corrosion Evaluation*, Elsevier, (1963) Amsterdam, Nederla nd.
9. A.J. Betts and L.H. Boulton, *Brit. Corros. J.*, 28 (1993) 279.
10. I. Alvarez-Armas and S. Degallaix-Moreuil, *Duplex Stainless Steels*, ISTE Ltd, (2009) London, En gland.
11. K. Fushimi, K. Takakura, H. Habazaki, H. Konno, K, Azumi and S. Tsuri, *ECS Transactions*, 16 (2 009) 291.
12. V.S. Moura, L.D. Lima, J.M. Pardal, A.Y. Kina, R.R.A. Corte and S.S.M. Tavares, *Mater. Charact* ., 59 (2008) 1127.
13. H.Y. Ha, M.H. Jang, T.H. Lee and J.O. Moon, *Corros. Sci.*, 89 (2014) 154.
14. L.G. Garfias-Mesias, J.M. Sykes and C.D.S. Tuck, *Corros. Sci*., 38 (1996) 1319.
15. L. Zhang, W. Zhang, Y. Jiang, B. Deng, D. Sun and J. Li, *Electrochim. Acta*, 54 (2009) 5387.
16. M. Liljas, P. Johansson, H.P. Liu and C.O.A. Olsson, *Steel. Res. Int*., 79 (2008) 466.
17. ASTM G61, *Standard Test Method for Conducting Cyclic Potentiodynamic Polarization Measure ments for Localized Corrosion Susceptibility of Iron-, Nickel-, or Cobalt-Based Alloys* (2003).
18. ASTM G5-14e1, *Standard Reference Test Method for Making Potentiodynamic Anodic Polarizatio n Measurements* (2004).
19. ASTM G78, *Standard Guide for Crevice Corrosion Testing of Iron-Base and Nickel-Base Stainless Alloys in Seawater and Other Chloride-Containing Aqueous Environments* (2015).
20. Q. Yu, C.F. Dong, Z.B. Liu, J.X. Liang, K. Xiao and X.G. Li, *Elec. Soc. S*., 10 (2015) 2035.
21. N.D. Cristofaro, M. Piantini and N. Zacchetti, *Corros. Sci*., 39 (1997) 2181.
22. N. Alonso-Falleiros, A. Hakim and S. Wolynec, *Corrosion*, 55 (1999) 443.
23. D. A. Jones, *Principles and prevention of corrosion*, Prentice Hall (2011) Upper saddle river, USA.
24. A. Prado, M.C. Merino, A.E. Coy, F. Viejo, R. Arrabal and E. Matykina, *Corrosion*, 50 (2008) 179 6.
25. Y. Yi, P. Cho, A. Al Zaabi and C. Jang, *Corros. Sci*., 74 (2013) 92.
26. Z. Szklarska-Smialowska, *Corros. Sci*., 41 (1999) 1743.
27. N. Pessall and C. Liu, *Electrochim. Acta*, 16 (1971) 1987.
28. X. He, B. Brettmann and H. Jung, *Corrosion*, 65 (2009) 449.
29. M.R. Ortiz, M.A. Rodriguez, R.M. Carranza and R.B. Rebak, *Corrosion*, 66 (2010) 1.
30. K.H. Kim, S.H. Lee, N.D. Nam and J.G. Kim, *Corros. Sci*., 53 (2011) 3576.
31. M.S. Hong, S.H. Kim, S.Y. Im and J.G. Kim, *Met. Mater. Int*., 22 (2016) 621.
32. M. Kissi, M. Bouklah, B. Hammouti and M. Benkaddour, *Appl. Surf. Sci*., 252 (2006) 4190.
33. A.S. Hamdy, E. El-Shenawy and T. El-Bitar, *Int. J. Electrochem. Soc*., 1 (2006) 171.
34. Y. Chen, T. Hong, M. Gopal and W.P. Jepson, *Corros. Sci*., 42 (2000) 979.
35. M.S. Hong, I.J. Park and J.G. Kim, *Met. Mater. Int*., 23 (2017) 708.
36. D.A. Lopez, S.N. Simison and S.R. De Sanchez, *Electrochim. Acta*, 48 (2003) 845.
37. F. Bentiss, M. Lebrini, H. Vezin, F. Chai and M. Lagrene, *Corros. Sci*., 51 (2009) 2165.
38. Y.T. Jeon and Y.S. Park, *J. Corros. Sci. Soc. of Kor*., 27 (1998) 384.
39. W.P. Yang, D. Coasta and P. Marcus, *J. Electrochem. Soc.*, 141 (1994) 111.
40. S. Fujimoto, W.S. Kim, M. Sato, J.Y. Son, M. Machida, K.T. Jung and H. Tsuchiya, *J. Solid State Electr.*, 19 (2015) 3512.
41. R.H. Jung, H. Tsuchiya and S. Fujimoto, *Corros. Sci.*, 58 (2013) 62.

42. Y.C. Lu and C.R. Clayton, *Corros. Sci*., 29 (1989) 927.
43. H. Luo, C.F. Dong, K. Xiao and X.G. Li, *Appl. Surf. Sci*., 258 (2011) 631.
44. E.D. Vito and P. Marcus, *Surf. Interface Anal*., 19 (1992) 403.
45. M. Kaneko and H.S. Isaacs, *Corros. Sci*., 44 (2002) 1825.
46. J. Shu, H. Bi, X. Li and Z. Xu, *Corros. Sci*., 57 (2012) 89.
47. A. Prado, M.C. Merino, A.E. Coy, F. Viejo, R. Arrabal and E. Matykina, *Corros. Sci*., 50 (2008) 7 80.
48. I. Olefjord, *Mater. Sci. Eng*., 42 (1980) 161.
49. I Olefjord, B. Brox and U. Jelvestam, *J. Electrochem. Soc*., 132 (1985) 2854.